Effect of the conductivity variations on computed electric field induced in learning-based models

Yinliang Diao, Essam A Rashed, Luca Giaccone, Ilkka Laakso, Congsheng Li, Riccardo Scorretti, Akimasa Hirata

IEEE Access
Multidisciplinary | Rapid Review | Open Access Journal

Date of publication xxxx 00, 0000, date of current version xxxx 00, 0000.

Digital Object Identifier 10.1109/ACCESS.2017.Doi Number

Effect of the conductivity variations on computed electric field induced in learning-based models

Yinliang Diao[1], (Member, IEEE), Essam A. Rashed[2], (Senior Member, IEEE), Luca Giaccone[3], (Senior Member, IEEE), Ilkka Laakso[4], (Member, IEEE), Congsheng Li[5], Riccardo Scorretti[6,7], and Akimasa Hirata[8,9], (Fellow, IEEE)

[1]College of Electronic Engineering, South China Agricultural University, Guangzhou 510642, China
[2]Graduate School of Information Science, University of Hyogo, Kobe 650-0047, Japan
[3]Dipartimento Energia "G. Ferraris", Politecnico di Torino, 10129 Torino, Italy
[4]Department of Electrical Engineering and Automation, Aalto University, 02150 Espoo, Finland
[5]China Academy of Information and Communications Technology, Beijing 100191, China
[6]Univ Lyon, CNRS, INSA Lyon, Université Claude Bernard Lyon 1, Ecole Centrale de Lyon, Ampère, UMR5005, 69622 Villeurbanne, France
[7]Department of Engineering, University of Perugia, 06125 Perugia, Italy
[8]Department of Electrical and Mechanical Engineering, Nagoya Institute of Technology, Nagoya 466-8555, Japan
[9]Center of Biomedical Physics and Information Technology, Nagoya Institute of Technology, Nagoya 466-8555, Japan

Corresponding author: Yinliang Diao (e-mail: diaoyinliang@ieee.org)

ABSTRACT Anatomical human models are extensively utilized for assessing induced electric fields due to low-frequency (LF) electromagnetic exposure. One difficulty in the LF dosimetry is that the results are often affected by numerical artifacts, which are attributable to the abrupt change at tissue interfaces for the segmented human models with discrete tissue conductivities. To overcome this difficulty, head models with continuous conductivities have been recently developed using deep learning networks, which directly map magnetic resonance images to volume conductivity without segmentation. To validate the effectiveness of this novel modeling method for electromagnetic dosimetry, a working group was established by the IEEE International Committee on Electromagnetic Safety Technical Committee 95 Subcommittee 6. The group's initial study focused on intercomparison of computed fields using learning-based models across several laboratories. This paper extends the analysis considering the effect of conductivity variations on the computed electric field induced in learning-based continuous models and segmented discrete models. Six international research groups participated in this joint study. It is found that the electric field strengths decrease in grey matter (GM) and increase in white matter (WM) as GM conductivity increases. Electric field strengths in both GM and WM decrease as WM conductivity increases. The variation ranges of electric field strength, due to varying conductivity values, show comparability between discrete and continuous models. For the intercomparison, the highest relative differences (RDs) are 15.9% and 6.7% for the 100th and 99th percentile values of the induced electric fields for the discrete models, respectively, and 10.1% and 3.8% for the continuous models. The RDs for computations using the scalar-potential finite-difference method with different solvers are below 1.2%.

INDEX TERMS Low frequency, electromagnetic safety, human protection, standardization, intercomparison study

I. INTRODUCTION

Concerns about human safety from electromagnetic (EM) exposure have long been prevalent. To address these concerns, the IEEE International Committee on Electromagnetic Safety (ICES) and the International Commission on Non-Ionizing Radiation Protection (ICNIRP) published standards [1] and guidelines [2], [3] establishing the exposure limits. These guidelines and standards are periodically updated to incorporate new scientific findings.

For low frequency (LF) exposure, the limits are designed to avoid electrostimulation effects to central or peripheral nervous system. There are two types of limits: basic restrictions (ICNIRP) or dosimetric reference limit (IEEE), and reference levels (ICNIRP) or exposure reference level

(IEEE). For LF exposure, basic restrictions are defined in terms of the spatially averaged induced electric field strength, derived from the threshold of adverse effects, electrostimulation for peripheral nervous system or sensation for central nervous system (phosphene), considering the reduction (safety) factor [3]. Reference levels are defined as permissible external electric or magnetic field strength in free space, which facilitates compliance assessment.

Reference levels are derived from basic restrictions to ensure that compliance with reference levels also ensures compliance with the basic restrictions. In the IEEE C95.1 standard, the exposure reference level was derived using homogeneous ellipses models [1], whereas in the ICNIRP guideline, realistic voxel-based human body models were used [4], [5], and an additional reduction factor of 3 was deemed in consideration of the uncertainty in the computations.

In many LF dosimetry studies [6]–[21], the utilized human models were developed based on tissue segmentation from medical images. A single conductivity value was then assigned to each tissue, so that the resulting volume conductor model is piecewise uniform. An important issue with the use of such discrete models for dosimetry modeling is the error caused by numerical artifacts, specifically the staircasing error [22]–[26]. Recently, head models with continuous conductivity have been developed using deep learning techniques and utilized for dosimetry [27], [28]. In these models, voxel conductivity was mapped from the gray levels of the original magnetic resonance images (MRIs), featuring smooth transition of conductivity across tissue interface [27].

Previous dosimetry studies primarily used conductivity values referenced in [4], [5], which were based on the Gabriel's dataset [29]. As reported by [30], the uncertainty in the measurement maybe up to a factor of 2 or 3 due to the electrode polarization effect below 100 Hz. For example, studies in [31], [32] reported higher tissue dielectric properties in brain tissues, note that their measurement methods, conditions and tissue temperatures were different [33]. Given the measurement uncertainty and variability in estimated tissue conductivity values, it is crucial to understand the effect of these variabilities on dosimetry modeling results [34]. Reference [35] considered three conductivity sets using 25 segmented head models, and the results showed that the maximum electric field strengths computed using the new tissue conductivities were lower than those obtained using commonly used conductivity values. Up to the best of authors' knowledge, there is no study that has yet examined the effect of conductivity variability for learning-based continuous head models. This gap underscores the need for further research to validate the effectiveness of these new modeling techniques in accounting for tissue conductivity variations.

International standardization bodies have highlighted the need for research on tissue conductivity assignment [36]. To address these issues, Subcommittee 6 of the IEEE ICES Technical Committee 95 launched a working group (WG7) focused on a novel modeling technique for LF dosimetry. That was the first study presenting an intercomparison using learning-based models to address computational uncertainties arising from different computational methods or codes. Seven worldwide institutions participated in that study. Five human head models were developed using CondNet [27], based on commonly used conductivity values. The induced electric fields were then computed using each group's individually developed computational codes, and the results showed good agreement across the various computations [37].

Following this, WG7 coordinated a second research effort to investigate how conductivity variations influence the computed electric field in the learning-based models. In this study, multiple conductivity sets for eight head models, with grey matter (GM) conductivity varying from 0.08 S/m to 0.22 S/m and white matter (WM) conductivity from 0.04 S/m to 0.14 S/m were generated using CondNet [27]. The cubically averaged electric fields in GM and WM were then computed for 50-Hz uniform magnetic field exposure. Additionally, different conductivity scenarios for a single head model were shared with WG7 members for an intercomparison study to verify the dosimetry results.

II. MODELS AND METHODS

A. MODELS AND SCENARIO

MRIs of eight subjects from the Brain Multimodality Dataset [38] were used to develop head models with a resolution of 1 mm × 1 mm × 1 mm. CondNet [27] was used for the automatic generation of the head models with continuous conductivity distributions, referred to as continuous models hereafter. This study considered the variety of GM and WM conductivities. TABLE I lists the tissue conductivities used for network training [39], with GM conductivity ranging from 0.08 S/m to 0.22 S/m and WM conductivity from 0.04 S/m to 0.14 S/m considering 0.02 S/m increments. Notably, GM conductivity was set to be higher than WM conductivity across the specified range. A total of 38 conductivity combinations were used for each head model, as shown in Table II. Additionally, segmented models with homogenous tissues were developed using ForkNet [40], referred to as discrete models hereafter. In summary, there are eight head models with a total of 608 simulation cases.

TABLE I
THE CONDUCTIVITIES OF THE MAJOR TISSUES USED FOR TRAINING CONDNET AT 50 HZ.

Tissue	Conductivity
Blood	0.70 S/m
Cancellous Bone	0.08 S/m
Cortical Bone	0.02 S/m
Cerebrospinal Fluid (CSF)	2.0 S/m
Cerebellum	0.095 S/m
Fat	0.04 S/m
Muscle	0.23 S/m
Skin	0.1 S/m
Grey Matter (GM)	0.08 ~ 0.22 S/m
White Matter (WM)	0.04 ~ 0.14 S/m

Figure 1 shows the conductivity distributions for one head model, showing that conductivity values varied smoothly in the continuous models compared to discrete head models. Figure 2 shows the distributions of the conductivity within two regions of interest (indicated by the red squares in Figure 1) for GM and WM. The medians, 0.122 S/m for GM and 0.042 S/m for WM, are close to the target tissue conductivities shown in Table II for scenario 6 (Sc6). Unlike the discrete models, where a single conductivity value is assigned to all voxels of a tissue, the voxel conductivity in learning-based continuous models is distributed around the median, reflecting the natural variability of conductivity in human tissues.

TABLE II
THE 38 SCENARIOS (SC) OF GM AND WM CONDUCTIVITY COMBINATIONS.

		GM Conductivity (S/m)							
		0.08	0.1	0.12	0.14	0.16	0.18	0.2	0.22
WM Conductivity (S/m)	0.04	Sc1	Sc3	Sc6	Sc10	Sc15	Sc21	Sc27	Sc33
	0.06	Sc2	Sc4	Sc7	Sc11	Sc16	Sc22	Sc28	Sc34
	0.08		Sc5	Sc8	Sc12	Sc17	Sc23	Sc29	Sc35
	0.1			Sc9	Sc13	Sc18	Sc24	Sc30	Sc36
	0.12				Sc14	Sc19	Sc25	Sc31	Sc37
	0.14					Sc20	Sc26	Sc32	Sc38

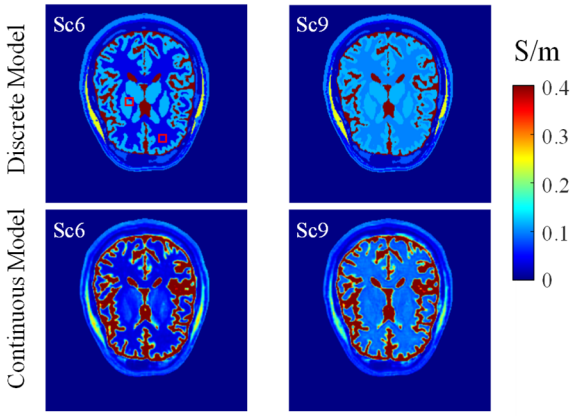

FIGURE 1. Distributions of the conductivity on the cross sections of continuous and discrete head model no. 4 at 50 Hz for conductivity scenarios 6 and 9.

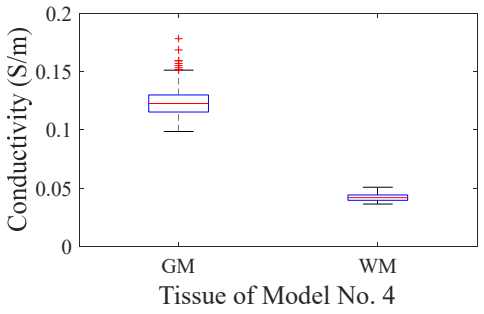

FIGURE 2. Boxplots showing voxel conductivity within regions of interest (6 × 6 × 6 voxels, indicated by the red squares in Fig. 1) for GM and WM.

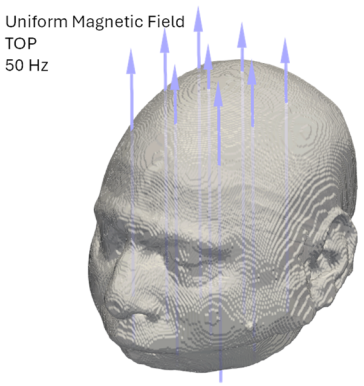

FIGURE 3. Illustration of the exposure scenario.

As shown in Figure 3, a uniform magnetic field of 200 μT at 50 Hz was utilized as the source, aligning with reference levels specified in the ICNIRP guidelines for the general public. The magnetic field was oriented from top to bottom (TOP direction), corresponding to the largest cross-sectional area in the axial plane of the truncated head models.

B. LF EM COMPUTATIONAL METHODS

The induced electric fields in both continuous and discrete voxel-based head models were computed based on the quasistatic approximation [41]–[43]. The scalar potentials ϕ for an external magnetic field were computed using the following equation:

$$\nabla \cdot [\sigma(-\nabla\phi - j\omega \boldsymbol{A}_0)] = 0, \quad (1)$$

where $\boldsymbol{A}_0$ and σ denoted the magnetic vector potential of the applied magnetic field and the tissue conductivity, respectively, ω was angular frequency. The electric field along the side of the voxel was obtained as follows:

$$\boldsymbol{E} = -\nabla\phi - j\omega \boldsymbol{A}_0. \quad (2)$$

The scalar-potential finite-difference (SPFD) method was utilized by a team from South China Agricultural University (SCAU) for computation of the induced electric field strengths in eight head models (both discrete and continuous) with all conductivity scenarios.

After computing the raw electric field at each voxel, the 8-mm^3 cubic spatial averaging was applied. Similar to the first study of WG7 [37], two averaging methods were considered. In method 1, all tissue types were allowed in the averaging cube, and averaging was performed over all voxels in the cube. In method 2, only the target tissue was allowed in the cube. If the averaging cube contained voxels from other tissues, averaging was not performed, and these voxels were excluded from the computations of percentile values. Then the 99th percentile values of the averaged electric field (E99) were obtained and compared.

C. INTERCOMPARISON OF RESULTS

For the intercomparison, one head model (both continuous and discrete) with 38 conductivity scenarios were shared with WG members. The SPFD method [6] was utilized by teams from the Nagoya Institute of Technology (NITech), and SCAU, each using their individual solver. Politecnico di Torino (PoliTO) also used SPFD, but with an algebraic framework [44], [45]. The finite element method (FEM) was utilized by Aalto University, CNRS/University of Perugia (Ampère), and China Academy of Information and Communications Technology (CAICT).

For FEM simulations, the same $A-\phi$ formulation as shown in (1) was adopted, where the nodal scalar potential is the unknown variable and the magnetic vector potential is derived from the uniform magnetic flux density. First-order cubical elements were utilized. The geometric multi-grid method for FEM was used by Aalto [46], and the aggregation-based algebraic multigrid solver was used by Ampère [45], [47]. The FEM solver of SEMCAD (version 19.2) [48] was used by CAICT for discrete models. The two averaging methods were implemented independently by each group.

The relative difference (RD) across the results of different groups was calculated as follows:

$$RD = \left|\frac{A_i - A_r}{A_r}\right| \times 100, \qquad (3)$$

where A_i denoted the results obtained by the i^{th} group, and A_r was the average of the results from all groups.

III. RESULTS

Figure 4 shows the maximum E99 in GM and WM across eight head models with varying GM and WM conductivities. The results obtained using averaging method 1 are shown in the upper four subfigures. For the continuous models, the maximum E99 in GM is 4.2 mV/m, and for the discrete models, it is 4.4 mV/m when $\sigma_{GM} = 0.08$ S/m and $\sigma_{WM} = 0.04$ S/m. In WM, the maximum E99 for the continuous model is 5.6 mV/m with $\sigma_{GM} = 0.2$ S/m and $\sigma_{WM} = 0.04$ S/m. The maximum E99 in WM for the discrete model is 5.6 mV/m but is observed with $\sigma_{GM} = 0.22$ S/m and σ_{WM} =0.04 S/m.

The E99 values of averaged electric field using method 2 are shown in the lower four subfigures. As expected, averaging method 2 produced slightly lower E99 values in both GM and WM. This reduction is due to the exclusion of more voxels in the computation of percentile values. Figure 5 presents the distributions of the mean E99 values across the eight head models, displaying similar trends to those in Figure 4, but with overall lower values.

A. Difference between Continuous and Discrete Models

As seen in Figures 4 and 5, the E99 values exhibit smooth and monotonic trends for the discrete models. However, for the continuous models, while the general tendencies are similar, some fluctuations can be observed, primarily due to the continuous distribution of tissue conductivity, especially near tissue interfaces.

The variation ranges for the continuous models are similar to or slightly narrower than those for the discrete models. For example, in the discrete models using averaging method 1, the maximum E99 values in GM across the eight head models range from 3.6 mV/m to 4.4 mV/m. In contrast, the E99 in GM for continuous models ranges from 3.6 mV/m to 4.2 mV/m, as

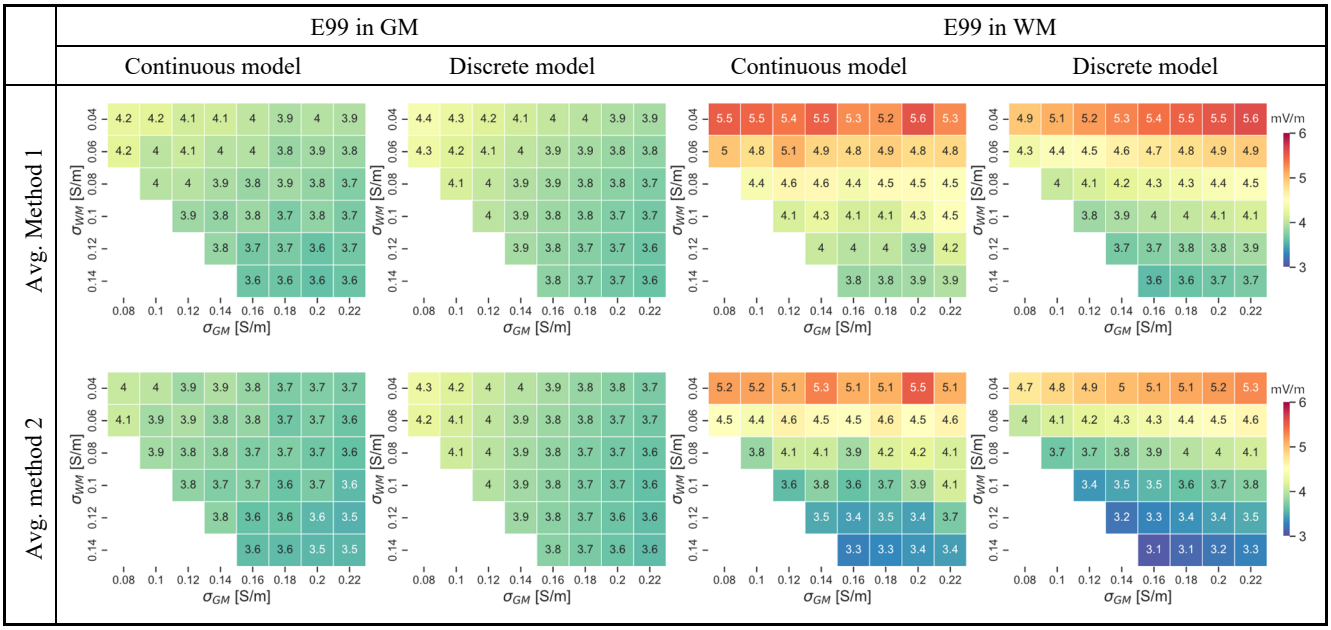

FIGURE 4. Heatmaps of the maximum 99$^{\text{th}}$ percentile values of the electric field strengths across eight head models with varying GM and WM conductivities.

This article has been accepted for publication in IEEE Access. This is the author's version which has not been fully edited and content may change prior to final publication. Citation information: DOI 10.1109/ACCESS.2024.3514710

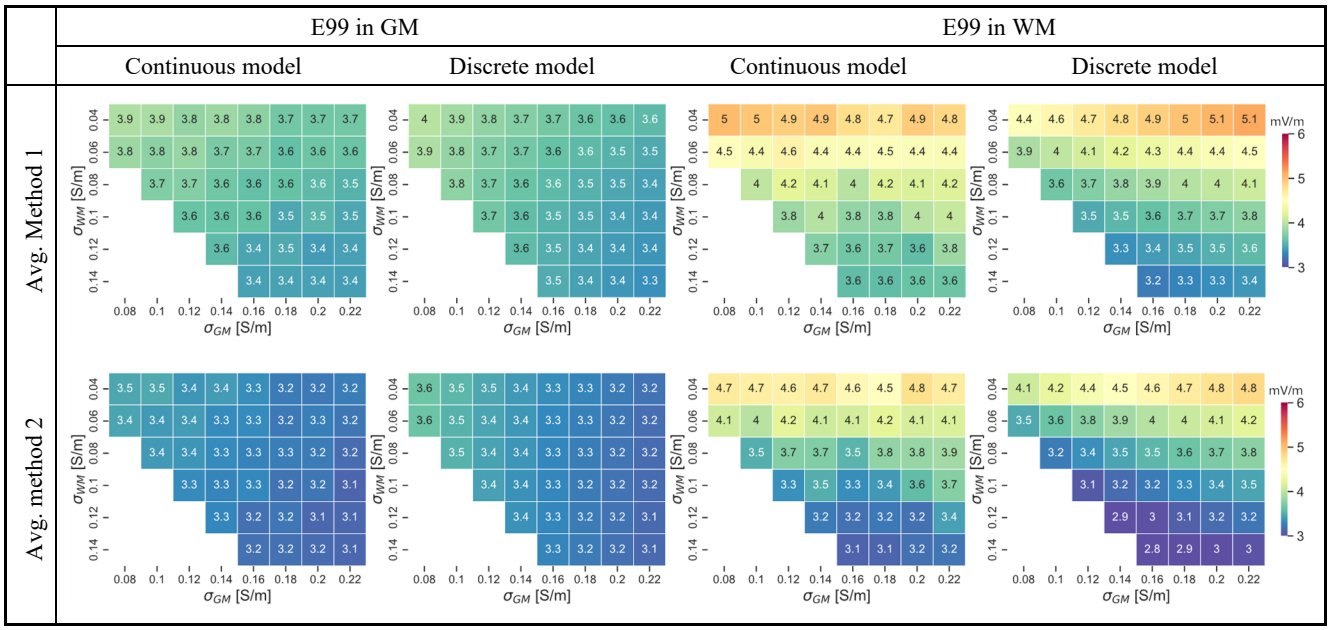

FIGURE 5. Heatmaps of the mean 99th percentile values of the electric field strengths across eight head models with varying GM and WM conductivities.

shown in Figure 4. This trend is also evident in Figure 5, which shows the mean E99 values across the eight head models.

Figure 6 shows the RDs in the E99 in GM and WM between continuous and discrete models, calculated as the difference of E99 in the continuous model from the discrete model, divided by their average value. As seen, the mean RDs for E99 in GM are below approximately 1% for both averaging methods, while those for E99 in WM are below 6%. The standard deviations of the RDs are about 2.4% for E99 in GM and 6.0% for WM, and these values are comparable across both averaging methods. The maximum RDs between the two types of models are approximately 9% for GM and 24% for WM, respectively. The E99 in WM of the continuous models are generally higher than those of the discrete models, likely due to the smoothing of conductivity contrast between GM and WM, resulting from the gradual transition of conductivity across the tissue interfaces in the continuous models.

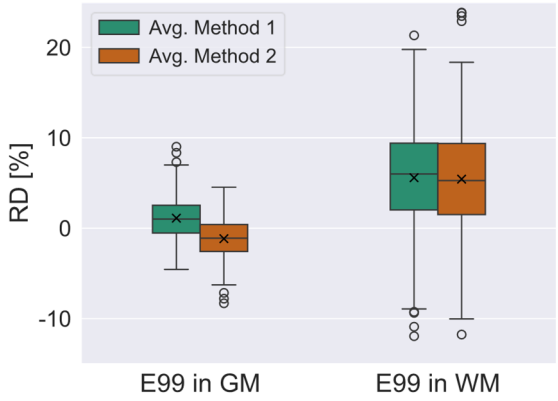

FIGURE 6. Boxplot of the relative differences in E99 in GM and WM between continuous and discrete models across all head models and scenarios. Horizontal bar in the box indicates the median, and the cross indicates the mean value.

B. Effect of GM Conductivity Variations

The general trends for the maximum and mean values of the electric field across the eight head models are illustrated in Figures 4 and 5. It was observed that E99 decreases in GM and increases in WM as GM conductivity increases. Conversely, E99 in both GM and WM decreases as WM conductivity increases.

Figure 7 specifically shows the changes in E99 in GM and WM as GM conductivity varies, with WM conductivity fixed at 0.06 S/m. It is observed that increasing GM conductivity leads to a slight decrease in E99 in GM. The reductions are approximately 6% and 11% for continuous and discrete head models, respectively, when GM conductivity increases from 0.08 S/m to 0.22 S/m. The effect on E99 in WM for continuous models is marginal, which is less than 3%. However, for discrete models, the effect leads to an increase of approximately 15% and 19% for averaging methods 1 and 2, respectively.

C. Effect of WM Conductivity Variations

Figure 8 illustrates the variation in E99 in GM and WM with changing WM conductivity, while maintaining GM conductivity at 0.16 S/m. An increase in WM conductivity results in a minor decrease in E99 values in GM, with reductions of less than approximately 10%. This effect is slightly more pronounced in continuous models compared to discrete models. In contrast, the effect of GM conductivity variation on E99 in WM is substantial for both model types.

Specifically, E99 in WM decreases by approximately 30% in the continuous models and 40% in discrete models as WM conductivity increases from 0.04 S/m to 0.14 S/m.

D. Intercomparison Results

Figure 9 illustrates the computed maximum averaged electric field strength (E100) and E99 in GM and WM across five

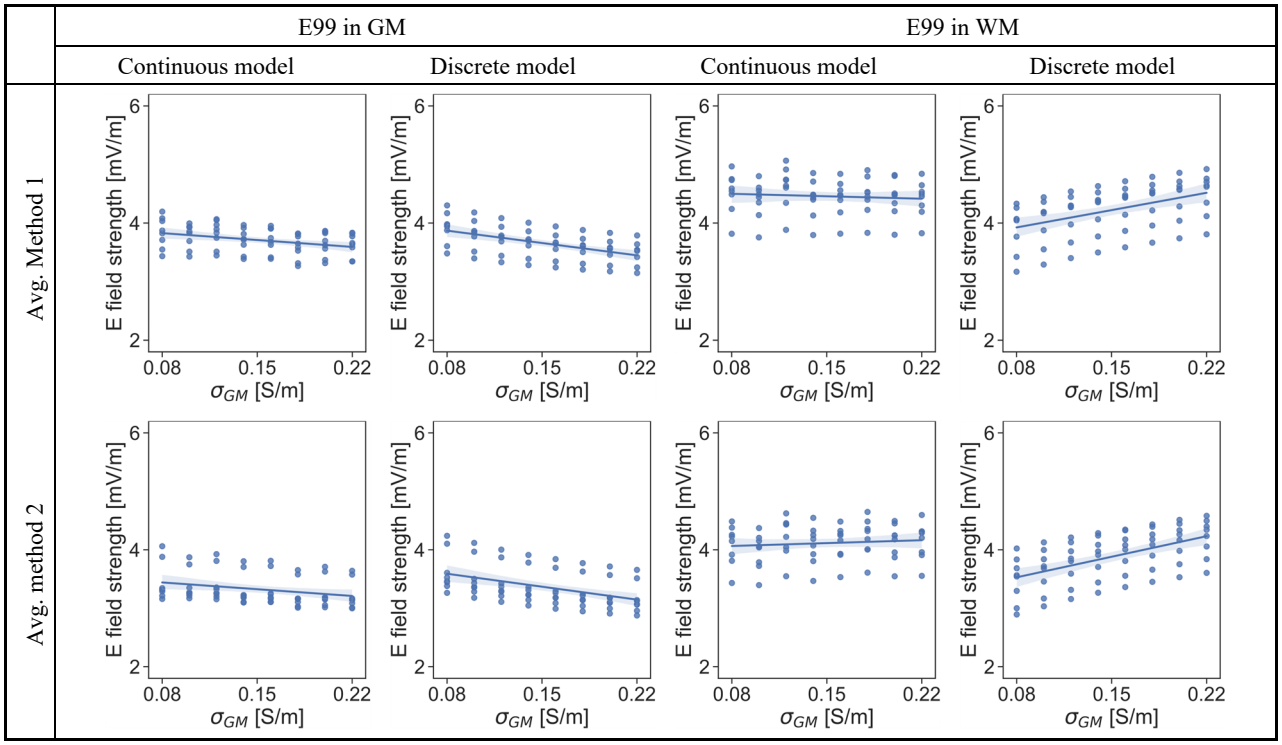

FIGURE 7. Effect of the varying GM conductivity on the E99 in GM and WM for both averaging methods, with WM conductivity fixed at 0.06 S/m.

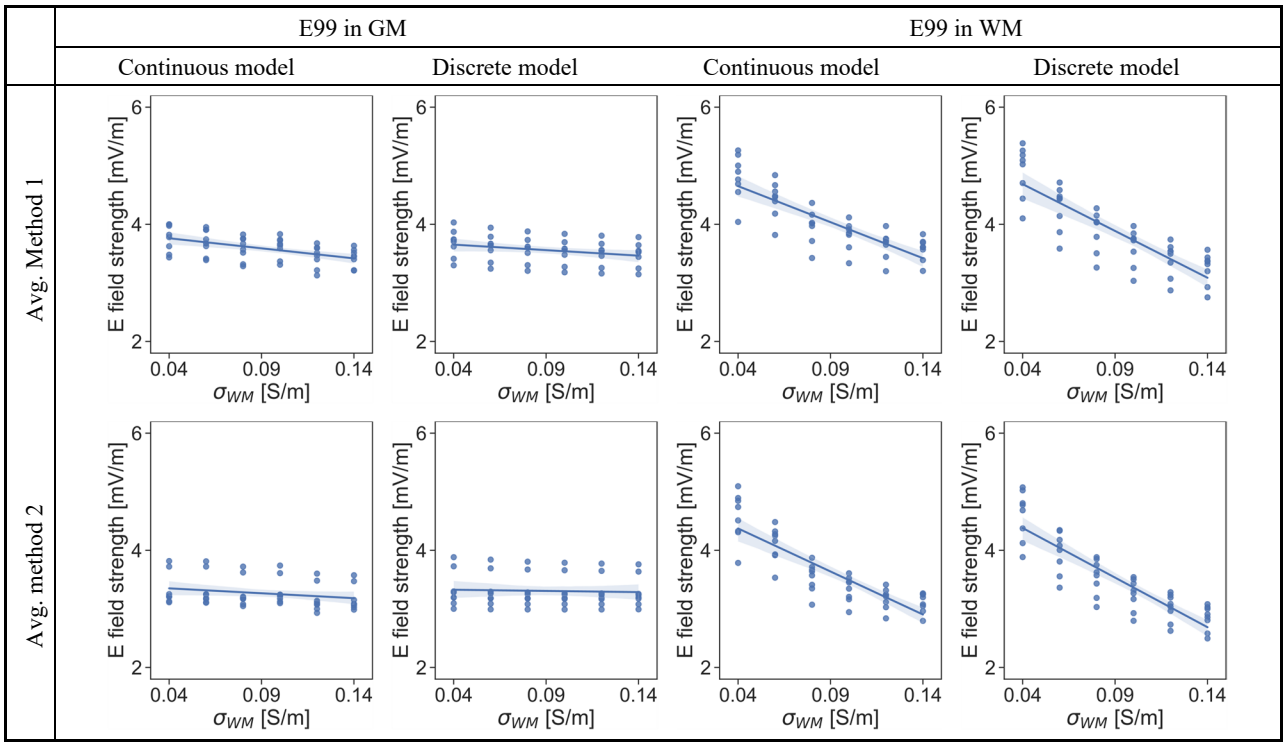

FIGURE 8. Effect of the varying WM conductivity on the E99 in GM and WM for both averaging methods, with GM conductivity fixed at 0.16 S/m.

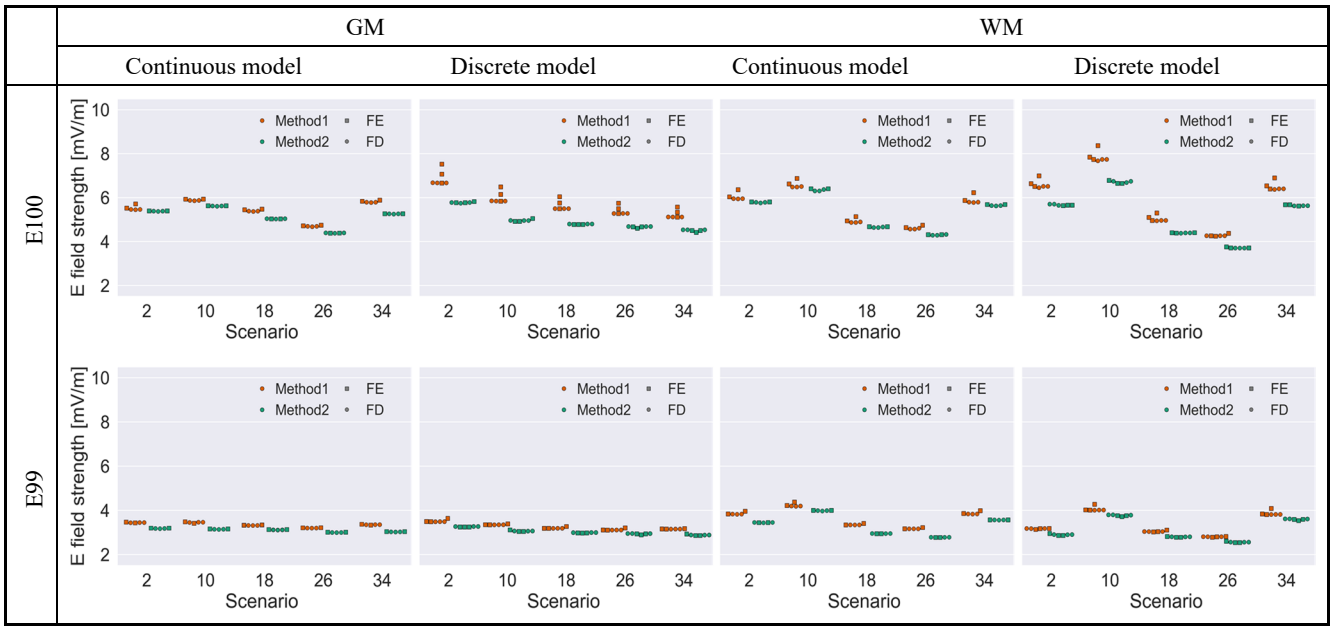

FIGURE 9. Intercomparison of the E100 and E99 in GM and WM computed using different codes from six research groups. The square and circular markers represent the results computed using FEM and SPFD methods, respectively.

selected scenarios for one head model. Good agreement among the six research groups is evident from the scatter points in the figure. The electric field strengths computed using the FEM are slightly higher than those calculated using the SPFD method, particularly in some cases for discrete models with the averaging method 1. These figures indicate that the RDs for E99 are generally lower than those for E100. Additionally, the RDs for the averaged electric fields using method 2 are consistently lower than those using method 1.

Tables III and IV list the maximum RDs of the computed E100 and E99 for all six groups. For averaging method 1, the maximum RDs are 15.9% and 6.7% for E100 and E99, respectively, both observed in the discrete models. The corresponding maximum RDs are 10.1% and 3.8% for the continuous models. For averaging method 2, the maximum RDs are 3.9% and 2.9% for E100 and E99, respectively, for discrete models. And they are 1.6% and 0.8% for continuous models.

Tables V and VI list the maximum RDs for three groups using the SPFD method with their individual solvers. Excellent agreement is observed, with RDs below 1.2% for E100 and below 0.5% for E99. The maximum RDs in electric fields in WM are slightly higher than those in GM. Differences in the electric fields computed using the SPFD method and FEM are primarily due to variations in the nodal schemes.

TABLE III
MAX RD IN E100 IN GM AND WM FOR ALL GROUPS.

Avg. Method	Model	E100 in GM	E100 in WM
1	Continuous	5.78%	10.11%
1	Discrete	9.58%	15.93%
2	Continuous	0.77%	1.59%
2	Discrete	3.90%	2.39%

TABLE IV
MAX RD IN E99 IN GM AND WM FOR ALL GROUPS.

Avg. Method	Model	E99 in GM	E99 in WM
1	Continuous	1.23%	3.75%
1	Discrete	3.46%	6.69%
2	Continuous	0.67%	0.77%
2	Discrete	2.93%	2.81%

TABLE V
MAX RD IN E100 IN GM AND WM FOR SPFD RESULTS.

Avg. Method	Model	E100 in GM	E100 in WM
1	Continuous	0.74%	1.19%
1	Discrete	0.82%	0.73%
2	Continuous	0.37%	1.19%
2	Discrete	0.46%	0.73%

TABLE VI
MAX RD IN E99 IN GM AND WM FOR SPFD RESULTS.

Avg. Method	Model	E99 in GM	E99 in WM
1	Continuous	0.22%	0.32%
1	Discrete	0.14%	0.16%
2	Continuous	0.36%	0.43%
2	Discrete	0.14%	0.25%

IV. DISCUSSION AND CONCLUDING REMARKS

Learning-based head models have recently been utilized in dosimetry studies for human protection from electromagnetic fields. To confirm the usability of such models for dosimetry analysis, the WG7 of IEEE ICES TC95 SC6 coordinated a study to investigate how conductivity variations influence the computed electric field in learning-based models. CondNet

was trained to generate eight head models with different tissue conductivity combinations. Specifically, GM conductivity ranged from 0.08 S/m to 0.22 S/m, and WM conductivity ranged from 0.04 S/m to 0.14 S/m. The other tissue conductivities were fixed, as reported in [35], the effect of non-brain tissues was marginal. A total of 38 tissue conductivity scenarios were created for each of the eight continuous and discrete head models. Additionally, an intercomparison study involving six research groups was conducted to validate computations using different computational methods or programs. To the best of our knowledge, this is the first study to investigate the effect of tissue conductivity variations for learning-based head models.

It was found that the increasing GM conductivity leads to a slight decrease in E99 in GM, but an increase in E99 in WM, due to the higher conductivity contrast between GM and WM. The effects of GM conductivity on E99 in brain tissues were less than 10% for both continuous and discrete head models. Conversely, E99 in GM and WM decreased as WM conductivity increased, with a reduction of 30 to 40% observed in WM, when WM conductivity changes from 0.04 S/m to 0.14 S/m.

The results show smoother changes of the E99 values for discrete models. However, for continuous models, fluctuations were observed, as shown in Figs. 4 and 5. This is because the CondNet needs to be trained separately for each conductivity scenario, making it challenging to harmonize the stop criterion for all scenarios. Nonetheless, the E99 values for the continuous models were comparable to or slightly lower than those for the discrete models, with mean RDs for E99 in GM being below 1% and those in WM below 6%. While continuous models show some fluctuations due to the smooth distribution of tissue conductivity, the variation ranges appear to be slightly narrower than those of discrete models. Overall, the choice between continuous and discrete models may not significantly affect the dosimetry results.

Considering all cases, the highest induced E99 in brain tissues were 28 mV/m and 27.5 mV/m per mT for averaging methods 1 and 2, respectively, in continuous models. In discrete models, these values were 28 mV/m and 26.5 mV/m, respectively. These values are observed at the highest GM to WM conductivity ratio. Compared to Sc2, which are similar to Gabriel's values, the highest increase was approximately 20% for continuous models and approximately 30% for discrete models. The value reported in [4] for magnetic field in TOP direction is 25.1 mV/m, thus the observed increase relative to this reference value is 12%.

For intercomparison of the results obtained by different methods and codes, the highest RD was found to be 15.9% between the use of the SPFD method and FEM, for E100 results obtained using averaging method 1. A possible explanation for this discrepancy is that the employed FEM formulation is equivalent to a minimization problem for the system's total coenergy, which must be numerically approximated. Due to unavoidable discretization errors, the computed coenergy is an approximation that tends to overestimate the true coenergy. This has also been observed in our previous study [37]. Another source of the RD might be attributable to staircasing artifacts associated with the implementation of the averaging methods. Because of the conductivity contrast between neighboring tissues, the electric field vectors are discontinuous across the tissue interface. Therefore, the RD in maximum electric field, which mainly appears in the voxels adjacent to tissue interfaces, might be amplified when different numerical solvers were used. For E99, the maximum RD was reduced to less than 7%. Furthermore, the RDs in the electric field computed using the SPFD method with different programs were reduced to below 1.2%.

In contrast, the RDs in the results caused by source and head modeling are marginal, since we have harmonized model and scenario parameters as much as possible. The stop criterion in terms of the residual norm may also affect the numerical computational accuracy. However, for head models with different resolutions, the relative error, defined in terms of the localized maximum electric field strength, is below 1% when the relative residual norm was set to be smaller than 10^{-5} for a localized exposure scenario [46], [49]. In our intercomparison, all groups were therefore asked to utilize a stop criterions of residual norm being smaller than 10^{-6}, this criterion has also been utilized in previous literature [12], [21], [50].

Based on the computational results, averaging method 2 seems to be more reliable than method 1, as it appears to be unaffected by the numerical methods. As illustrated Tables III to VI, the RDs in both E99 and E100 using method 2 are typically smaller than those computed using method 1, as the latter included electric field strengths in voxels belonging to other tissues. Additionally, the differences between the continuous and discrete head models (Fig. 6) are smaller for method 2 than for method 1.

In summary, these RDs reported in this study are substantially smaller than the reduction factor of 3 used before. The results of this study could be informative for future revisions of the international guidelines or standards.

APPENDIX

The source code of CondNet is available in Mathematica (https://github.com/erashed/CondNet) and Python (https://github.com/rrwabina/condnet).

ACKNOWLEDGMENT

The authors would like to thank Dr. Kensuke Sasaki (National Institute of Information and Communications Technology, Tokyo, Japan) for valuable discussion on tissue dielectric properties and support for working group activities.

REFERENCES

[1] IEEE C95.1-2019, *IEEE Standard for Safety Levels with Respect to Human Exposure to Electric, Magnetic and Electromagnetic Fields, 0 Hz to 300 GHz*. NY, USA, 2019.

[2] ICNIRP, "Guidelines for limiting exposure to electromagnetic fields (100 kHz to 300 GHz)," *Health Phys.*, vol. 118, no. 5, pp. 483–524, 2020.
[3] ICNIRP, "Guidelines for limiting exposure to time-varying electric and magnetic fields (1 Hz to 100 kHz).," *Health Phys.*, vol. 99, no. 6, pp. 818–36, 2010.
[4] P. Dimbylow, "Development of the female voxel phantom, NAOMI, and its application to calculations of induced current densities and electric fields from applied low frequency magnetic and electric fields," *Phys. Med. Biol.*, vol. 50, no. 6, p. 1047, 2005.
[5] P. Dimbylow, "Development of pregnant female, hybrid voxel-mathematical models and their application to the dosimetry of applied magnetic and electric fields at 50 Hz," *Phys. Med. Biol.*, vol. 51, no. 10, p. 2383, 2006.
[6] T. W. Dawson, K. Caputa, and M. A. Stuchly, "High-resolution organ dosimetry for human exposure to low-frequency electric fields," *IEEE Trans. Power Deliv.*, vol. 13, no. 2, p. 366, 1998.
[7] A. Hirata, K. Caputa, T. W. Dawson, and M. A. Stuchly, "Dosimetry in models of child and adult for low-frequency electric field," *IEEE Trans. Biomed. Eng.*, vol. 48, no. 9, pp. 1007–1012, 2001.
[8] C. Li and T. Wu, "Dosimetry of infant exposure to power-frequency magnetic fields: Variation of 99th percentile induced electric field value by posture and skin-to-skin contact," *Bioelectromagnetics*, vol. 36, no. 3, pp. 204–218, 2015.
[9] R. P. Findlay, "Induced electric fields in the Maxwell surface-based human model from exposure to external low frequency electric fields," *Radiat. Prot. Dosimetry*, vol. 162, no. 3, pp. 244–253, 2014.
[10] X. Chen *et al.*, "Analysis of human brain exposure to low-frequency magnetic fields: A numerical assessment of spatially averaged electric fields and exposure limits," *Bioelectromagnetics*, vol. 34, no. 1, pp. 375–384, 2013.
[11] G. Schmid and R. Hirtl, "On the importance of body posture and skin modelling with respect toin situelectric field strengths in magnetic field exposure scenarios," *Phys. Med. Biol.*, vol. 61, no. 12, pp. 4412–4437, May 2016.
[12] Y. Takahashi, A. Ahagon, K. Fujiwara, T. Iwashita, and H. Nakashima, "Analysis of induced electric field in human body by utility power frequency magnetic field using parallel fast multipole-accelerated boundary element method," *IET Sci. Meas. Technol.*, vol. 9, no. 2, pp. 178-183(5), Mar. 2015.
[13] I. Liorni *et al.*, "Dosimetric study of fetal exposure to uniform magnetic fields at 50 Hz," *Bioelectromagnetics*, vol. 35, no. 8, pp. 580–597, 2014.
[14] J. Chakarothai, K. Wake, T. Arima, S. Watanabe, and T. Uno, "Exposure evaluation of an actual wireless power transfer system for an electric vehicle with near-field measurement," *IEEE Trans. Microw. Theory Tech.*, vol. 66, no. 3, pp. 1543–1552, Mar. 2018.
[15] K. Taguchi *et al.*, "Relationship of external field strength with local and whole-body averaged specific absorption rates in anatomical human models," *IEEE Access*, vol. 6, pp. 70186–70196, 2018.
[16] K. Wake *et al.*, "Derivation of coupling factors for different wireless power transfer systems: Inter-and intralaboratory comparison," *IEEE Trans. Electromagn. Compat.*, vol. 59, no. 2, pp. 677–685, 2017.
[17] A. Arduino *et al.*, "Accuracy assessment of numerical dosimetry for the evaluation of human exposure to electric vehicle inductive charging systems," *IEEE Trans. Electromagn. Compat.*, vol. 62, no. 5, pp. 1939–1950, Oct. 2020.
[18] M. A. Stuchly and O. P. Gandhi, "Inter-laboratory comparison of numerical dosimetry for human exposure to 60 Hz electric and magnetic fields," *Bioelectromagnetics*, vol. 21, no. 3, pp. 167–174, 2000.
[19] A. Hirata *et al.*, "Intercomparison of induced fields in Japanese male model for ELF magnetic field exposures: effect of different computational methods and codes," *Radiat. Prot. Dosimetry*, vol. 138, no. 3, pp. 237–244, 2010.
[20] K. Aga *et al.*, "Intercomparison of in situ electric fields in human models exposed to spatially uniform magnetic fields," *IEEE Access*, vol. 6, pp. 70964–70973, 2018.
[21] P. Lagouanelle, F. Freschi, L. Pichon, and L. Giaccone, "Fast and reliable human exposure assessment around high power systems using surrogate modeling," *IEEE Access*, vol. 12, pp. 34835–34845, 2024.
[22] A. Conchin Gubernati, F. Freschi, L. Giaccone, and R. Scorretti, "Analysis of numerical artifacts using tetrahedral meshes in low frequency numerical dosimetry," *Applied Sciences*, vol. 12, no. 13. 2022.
[23] M. Soldati and I. Laakso, "Computational errors of the induced electric field in voxelized and tetrahedral anatomical head models exposed to spatially uniform and localized magnetic fields," *Phys. Med. Biol.*, vol. 65, p. 015, 2020.
[24] Y. Diao, L. Liu, N. Deng, S. Lyu, and A. Hirata, "Tensor-conductance model for reducing the computational artifact in target tissue for low-frequency dosimetry," *Phys. Med. Biol.*, vol. 68, no. 20, p. 205014, Oct. 2023.
[25] Y. Diao, L. Zhang, D. Shi, and A. Hirata, "An effective edge conductivity for reducing staircasing error in induced electric field computation for low-frequency magnetic field dosimetry," *Phys. Med. Biol.*, vol. 67, no. 21, p. 215011, Oct. 2022.
[26] J. P. Reilly and A. Hirata, "Low-frequency electrical dosimetry: research agenda of the IEEE International Committee on Electromagnetic Safety," *Phys. Med. Biol.*, vol. 61, no. 12, p. R138, 2016.
[27] E. A. Rashed, J. Gomez-Tames, and A. Hirata, "Deep learning-based development of personalized human head model with non-uniform conductivity for brain stimulation," *IEEE Trans. Med. Imaging*, vol. 39, no. 7, pp. 2351–2361, 2020.
[28] Y. Diao, E. A. Rashed, and A. Hirata, "Induced electric field in learning-based head models with smooth conductivity for exposure to uniform low-frequency magnetic fields," *IEEE Trans. Electromagn. Compat.*, vol. 64, no. 6, pp. 1969–1977, 2022.
[29] C. Gabriel, *Compilation of the Dielectric Properties of Body Tissues at RF and Microwave Frequencies.* Brooks Air Force Base, RFR Division, San Antonio, TX, Final Tech. Rep. Occupational and Environmental Health Directorate AL/OE-TR-1996-0037, 1996.
[30] S. Gabriel, R. W. Lau, and C. Gabriel, "The dielectric properties of biological tissues: II. Measurements in the frequency range 10 Hz to 20 GHz," *Phys. Med. Biol.*, vol. 41, no. 11, p. 2251, 1996.
[31] G. Schmid, G. Neubauer, and P. R. Mazal, "Dielectric properties of human brain tissue measured less than 10 h postmortem at frequencies from 800 to 2450 MHz," *Bioelectromagnetics*, vol. 24, no. 6, pp. 423–430, Sep. 2003.
[32] J. Latikka, T. Kuurne, and H. Eskola, "Conductivity of living intracranial tissues," *Phys. Med. Biol.*, vol. 46, no. 6, p. 1611, 2001.
[33] K. Sasaki, E. Porter, E. A. Rashed, L. Farrugia, and G. Schmid, "Measurement and image-based estimation of dielectric properties of biological tissues —past, present, and future—," *Phys. Med. & Biol.*, vol. 67, no. 14, p. 14TR01, 2022.
[34] A. Hirata *et al.*, "Assessment of human exposure to electromagnetic fields: review and future directions," *IEEE Trans. Electromagn. Compat.*, vol. 63, no. 5, pp. 1619–1630, 2021.
[35] M. Soldati and I. Laakso, "Effect of electrical conductivity uncertainty in the assessment of the electric fields induced in the brain by exposure to uniform magnetic fields at 50 Hz," *IEEE Access*, vol. 8, pp. 222297–222309, 2020.
[36] ICNIRP, "Gaps in knowledge relevant to the 'guidelines for limiting exposure to time-varying electric and magnetic fields (1 Hz-100 kHz),'" *Health Phys.*, vol. 118, no. 5, pp. 533–542, 2020.
[37] Y. Diao *et al.*, "Intercomparison of the averaged induced electric field in learning-based human head models exposed to low-frequency magnetic fields," *IEEE Access*, vol. 11, no. March, pp. 38739–38752, 2023.
[38] "MIDAS - Collection NAMIC: Brain Mutlimodality." [Online]. Available: http://insight-journal.org/midas/collection/view/190. [Accessed: 22-Apr-2020].
[39] S. Gabriel, R. W. Lau, and C. Gabriel, "The dielectric properties of biological tissues: III. Parametric models for the dielectric spectrum of tissues," *Phys. Med. Biol.*, vol. 41, no. 11, pp. 2271–2293, 1996.
[40] E. A. Rashed, J. Gomez-Tames, and A. Hirata, "End-to-end semantic segmentation of personalized deep brain structures for non-invasive brain stimulation," *Neural Networks*, vol. 125, pp. 233–244, 2020.
[41] A. Hirata, F. Ito, and I. Laakso, "Confirmation of quasi-static approximation in SAR evaluation for a wireless power transfer system.," *Phys. Med. Biol.*, vol. 58, no. 17, pp. N241-249, 2013.
[42] A. Barchanski, H. De Gersem, E. Gjonaj, and T. Weiland, "Impact of the displacement current on low-frequency electromagnetic fields

computed using high-resolution anatomy models," *Phys. Med. Biol.*, vol. 50, no. 19, pp. N243--N249, 2005.
[43] S. W. Park, K. Wake, and S. Watanabe, "Calculation errors of the electric field induced in a human body under quasi-static approximation conditions," *IEEE Trans. Microw. Theory Tech.*, vol. 61, no. 5, pp. 2153–2160, 2013.
[44] F. Freschi, L. Giaccone, V. Cirimele, and A. Canova, "Numerical assessment of low-frequency dosimetry from sampled magnetic fields," *Phys. Med. Biol.*, vol. 63, no. 1, p. 15029, 2017.
[45] Y. Notay, "An aggregation-based algebraic multigrid method," *Electron. Trans. Numer. Anal.*, vol. 37, no. 6, pp. 123–146, 2010.
[46] I. Laakso and A. Hirata, "Fast multigrid-based computation of the induced electric field for transcranial magnetic stimulation," *Phys. Med. Biol.*, vol. 57, no. 23, pp. 7753–7765, 2012.
[47] R. Scorretti, R. V Sabariego, L. Morel, C. Geuzaine, N. Burais, and L. Nicolas, "Computation of induced fields into the human body by dual finite element formulations," *IEEE Trans. Magn.*, vol. 48, no. 2, pp. 783–786, 2012.
[48] *SEMCAD version 19.2*. (2021). speag. [Online]. Available: https://speag.swiss/products/semcad/solutions/.
[49] M. Soldati, "Characterization of open issues in low-frequency computational dosimetry." Aalto University, 2021.
[50] M. Soldati, T. Murakami, and I. Laakso, "Inter-individual variations in electric fields induced in the brain by exposure to uniform magnetic fields at 50 Hz," *Phys. Med. & Biol.*, vol. 65, no. 21, p. 215006, Oct. 2020.

YINLIANG DIAO (S'12–M'17) received the B. E. degree in electronic information engineering from Chongqing University, Chongqing, China, in 2008, the M.S. degree in electronic engineering from the Beijing University of Posts and Telecommunications, Beijing, China, in 2011, and the Ph.D. degree in electronic engineering from the City University of Hong Kong, in 2016.

Since 2017, he has been with the College of Electronic Engineering at South China Agricultural University in Guangzhou, China, initially as an Assistant Professor and currently serving as an Associate Professor. In 2019, he also joined the Department of Electrical and Mechanical Engineering at Nagoya Institute of Technology, where he is currently a Guest Associate Professor. His research interests include electromagnetic dosimetry modeling and electromagnetic compatibility.

Dr. Diao is a co-chair of Subcommittee 6 of IEEE International Committee on Electromagnetic Safety TC-95, and a member of the Scientific Expert Group of International Commission on Non-Ionizing Radiation Protection. He was a recipient of the Young Scientist Award from URSI GASS 2020.

ESSAM A. RASHED (M'11–SM'19) received the Ph.D. (Eng.) degree in computer science from the University of Tsukuba, Tsukuba, Japan, in 2010. From 2010 to 2012, he was a JSPS Research Fellow with the University of Tsukuba. He served as an Assistant/Associate/Full Professor of Computer Science with the Department of Mathematics, Faculty of Science, Suez Canal University. From 2018 to 2021, he was a Research Professor with Nagoya Institute of Technology, Japan. He is currently a Professor with the Graduate School of Information Science, University of Hyogo, Kobe, Japan. His research interests include medical image processing, data science, artificial intelligence, and pattern recognition. Dr. Rashed is an Associate Editor for the IEEE Access. In 2024, he was a recipient of the commendation for Science and Technology (Development Category) by the Minister of MEXT, Japan. He participated as a PI and CoI for several external funded projects.

LUCA GIACCONE (M'14–SM'15) was born in Cuneo, Italy, in 1980. He received the Laurea and Ph.D. degrees in electrical engineering from the Politecnico di Torino, Turin, Italy, in 2005 and 2010, respectively. He works on several areas of the electrical engineering: optimization, modeling of complex energy systems, computation of electromagnetic and thermal fields, energy scavenging, magnetic field mitigation, EMF dosimetry, and compliance of LF pulsed magnetic field sources. Since 2017, he has been an Associate Professor with the Dipartimento Energia "G: Ferraris", Politecnico di Torino. Since 2015 he has been a member of the IEEE International Committee on Electromagnetic Safety—Technical Committee 95 - SC6 - dosimetry modeling. Since September 2017 he has been member of the National Italian Committee CEI-106 dealing with human exposure to electromagnetic fields. In 2020 Luca Giaccone was appointed as Member of the ICNIRP Scientific Expert Group (SEG).

ILKKA LAAKSO (M'14) received the M.Sc.(Tech.) degree in electromagnetics and circuit theory from Helsinki University of Technology, Espoo, Finland, in 2007, and the D.Sc.(Tech.) degree in electromagnetics from Aalto University, Espoo, Finland in 2011. Between 2013 and 2015, he was a Research Assistant Professor and a Research Associate Professor at the Department of Computer Science and Engineering, Nagoya Institute of Technology. Since 2015, he has been an Assistant Professor and since 2023 an Associate Professor at Aalto University. His research interest include computational bioelectromagnetic modeling for assessment of human safety and biomedical applications. He is the author of more than 100 papers published in international journals and conference proceedings. Dr. Laakso received several awards, including the Ericsson Young Scientist Award, 2011; the Young Scientist Award in URSI General Assembly and Scientific Symposium, Montreal, Canada, 2017, and the IEEE Electromagnetic Compatibility Society Technical Achievement Award for contribution to computational dosimetry of human exposure to electromagnetic fields from low frequencies to millimeter waves, 2021. He

is a member of the IEEE International Committee on Electromagnetic Safety and a member of the International Commission on Non-ionizing Radiation Protection.

CONGSHENG LI received the B.S. degree in electronic information engineering from Beijing City University, Beijing, China, in 2009, M.S. degree in signal and information system from Beijing Information Science and Technology University, Beijing, China, in 2012 and the Ph.D. degree from University of Science and Technology Beijing, China, in 2015.

From 2015 to now, he was an engineer and senior engineer with China Academy of Information and Communications Technology, Beijing, China. His research interest s include computational electromagnetics and artificial intelligence.

RICCARDO SCORRETTI was born in Prato, Italy in 1973. He received his Laurea (aka M.S. degree) in informatics engineering from Florence University, Italy, in 1999, and his Ph.D. degrees in electrical engineering from Ecole Centrale de Lyon, France, in 2003.

In 2005, he joined the National Council of Scientific Research at Laboratoire Ampère – UMR 5005 CNRS, Lyon, France. He is currently visiting scientist at the University of Perugia, Italy. In 2009 and 2019 he was a visiting scientist respectively at the Institut Montefiore, University of Liège, Belgium and Nagoya Institute of Technology, Japan. Since 2022 he has been a member of the IEEE International Committee on Electromagnetic Safety—Technical Committee 95 - SC6 - dosimetry modeling.

His research focus on computational electromagnetism, including modeling of hysteresis in magnetic materials and numerical dosimetry of electromagnetic fields.

AKIMASA HIRATA (S'98–M'01–SM'10–F'17) received the B.E. and M.E. degrees in in communications engineering from Osaka University, Suita, Japan, in 1996, 1998, and 2000, respectively.

From 1999 to 2001, he was a Research Fellow of the Japan Society for the Promotion of Science, and a Visiting Research Scientist at the University of Victoria, Victoria, BC, Canada, in 2000. In 2001, he joined the Department of Communications Engineering, Osaka University, as an Assistant Professor. In 2004, he joined, as an Associate Professor, the Department of Computer Science and Engineering, Nagoya Institute of Technology, where he is currently a Full Professor. His research interests include electromagnetic safety, risk management system for heat-related illness, methods in neuroscience, antennas, filters, and related computational techniques.

Prof. Hirata is an editorial board member of physics in medicine and biology, an associate editor of IEEE TRANSACTIONS ON ELECTROMAGNETIC COMPATIBILITY, a Chair of International Commission on Non-Ionizing Radiation Protection, and a Subcommittee (EMF Dosimetry Modeling) Chair of IEEE International Committee on Electromagnetic Safety, and an expert of World Health Organization. From 2006 to 2012, he was also an Associate Editor of the IEEE TRANSACTIONS ON BIOMEDICAL ENGINEERING. He received several awards including Young scientists' Prize (2006) and Prizes for Science and Technology (Research Category in 2011, Public Understanding Promotion Category in 2014, 2020, development Category 2024) by the Commendation for Science and Technology by the Minister of Education, Culture, Sports, Science, and Technology, Japan, and IEEE EMC-S Technical Achievement Award (2015) and the Richard R. Stoddart Award (2023), the Japan Academy Medal and JSPS Prize (2018), and Japan Open Innovation Prize (President of the Science Council of Japan Prize in 2022) from the Cabinet Office. He is a Fellow of Institute of Physics, and a member of IEICE, IEE Japan, and Bioelectromagnetics Society.